Dynamic Oxidation Behavior of TD-NiCr Alloy with Different Surface Pretreatments

C. T. YOUNG, D. R. TENNEY, AND H. W. HERRING

Oxidation tests of TD-NiCr alloy with different surface pretreatments were conducted in a Mach-5 arc-jet at 1200°C and 0.002 lb/s flowing air environment. Extensive scanning electron microscopy and X-ray analyses were carried out to determine the mechanisms responsible for the observed oxidation behavior. The presence of atomic oxygen in the air stream plays a significant role in determining the oxidation characteristic of the alloy. The rate of Cr_2O_3 vaporization by formation of volatile CrO_3 is greatly enhanced by the flowing conditions. The typical microstructure of oxides formed in the dynamic tests consists of an external layer of NiO with a porous "mushroom"-type morphology, an intermediate layer of NiO and Cr_2O_3 oxide mixture, and a continuous inner layer of Cr_2O_3 in contact with the Cr-depleted alloy substrate. The formation of mushroom-type NiO is attributed to three basic processes: 1) vaporization of NiO by dissociation into its elements, 2) reoxidation of Ni vapor predominantly with atomic oxygen, and 3) condensation of NiO at elevated sites on the specimen surface. The oxidation rate is determined by the rate of vaporization of NiO. Surface pretreatment has a significant effect on the oxidation behavior of the alloy in the early stage of oxidation, but becomes less important as exposure time increases. Mechanical polishing induces surface recrystallization, which enhances the formation of Cr_2O_3 in static environment, but promotes the concurrence of external growth of NiO and internal oxidation of the alloy in the dynamic atmosphere.

BECAUSE of its reported high strength and good static oxidation resistance at high temperature,[1-10] Ni-20 pct Cr-2 pct ThO_2 alloy, supplied under the trade name of TD-NiCr, has been considered for use in advanced jet engines and as a part of a thermal protection system for the space shuttle. The addition of submicron ThO_2 particles to the Ni-Cr alloy inhibits grain growth and stabilizes the substructure of the alloy, thereby retaining high strength at elevated temperature.[1-4] The addition of thoria particles also improves static oxidation resistance by promoting the selective oxidation of Cr to form protective Cr_2O_3, and by decreasing the growth rate of Cr_2O_3.[6-9] Surface preparation has a significant influence on the oxidation behavior of the alloy. Surface grinding enhances the formation of Cr_2O_3 whereas electropolishing promotes the formation of external NiO and inner Cr_2O_3 subscale.[8-12]

Under high temperature, high speed flowing gas conditions, a substantial increase in the oxidation rate has been observed as compared with the results of static testing. Gilbreath[13,14] has emphasized the importance of atomic oxygen which existed in the reentry environment, and has demonstrated the accelerated degradation of the alloy in dissociated oxygen. Lowell *et al*[15] has indicated that the loss rate of material in a 1-atmosphere, Mach-1 turbine gas stream at 1200°C was approximately 100 times greater than that of static tests. Enhanced oxidation in a Mach-1 burner gas stream at 1093°C was also observed by Johnston *et al*.[16] Centolenzi *et al*[17,18] has reported increased oxidation in a Mach-5 arc-jet gas stream, but no detailed mechanism has been given.

The oxidation behavior of TD-NiCr (belt-sanded surface finishing) in a Mach-5 arc-jet at 1200°C was reported in a preceding paper.[19] It was demonstrated that the external Cr_2O_3 formed during a static preoxidation was not stable in the high speed gas flow and was rapidly replaced by a layer of NiO with a porous mushroom-type morphology. In that work, metal recession was measured. The substrate thickness decreased rapidly at the early stages of oxidation, and decreased linearly with time at a much slower rate in the later stages of oxidation. A model was proposed to explain the observed oxidation behavior. To further confirm this proposed model, a comprehensive metallographic analysis of the oxidation characteristics of specimens having four different surface pretreatments was investigated in the present study. Oxidation tests were conducted, with emphasis being placed on short time tests where the effect of the original surface condition should be of most importance. The chronology of oxidation for each surface preparation and test time was fully documented. The data thus collected was combined with that reported earlier, to provide a better characterization of the oxidation behavior of TD-NiCr under simulated shuttle reentry conditions.

EXPERIMENTAL PROCEDURES

The TD-NiCr specimens used in this study were prepared from the same 0.02 in. thick sheet stock as that reported in the previous paper;[19] the sheet stock was received in a recrystallized condition, with a belt-sanded surface finish. The previous paper also describes the specimen configuration and alloy microstructure. To reveal the effect of surface pre-

C. T. YOUNG is with Bendix Research Laboratories, The Bendix Corporation, Southfield, MI 48076. D. R. TENNEY is with NASA-Langley Research Center, Hampton, VA 23665. H. W. HERRING is with NASA-Marshall Flight Center, Huntsville, AL 35812. C. T. Young and H. W. Herring were formerly Research Fellow and Materials Engineer, respectively, NASA-Langley Research Center, Hampton, VA. D. R. Tenney was formerly Assistant Professor of Metallurgical Engineering, Division of Mineral Engineering, Virginia Polytechnic Institute and State University, Blacksburg, VA.

Manuscript submitted February 15, 1974.

treatment on the oxidation behavior, specimens were given four different surface treatments prior to dynamic oxidation tests. These were: 1) electropolishing (EP), 2) mechanical polishing (MP), 3) electropolishing followed by static preoxidation (EP + PO), and 4) mechanical polishing followed by static preoxidation (MP + PO). MP was finished through 400 grit SiC abrasive paper. EP was carried out in a solution of 87 ml methanol, 8 ml H_2SO_4, 3 ml HNO_3, and 2 ml HF at room temperature and 17 V for 2 min. PO was conducted in air at 1100°C for 1 h.

Dynamic oxidation tests were conducted in a Mach-5 arc-jet operated with a mass flow of 0.002 lb/s air. Details on the arc-heater equipment have been given in the previous paper.[19] The power to the arc-heater was adjusted to yield a gas temperature sufficient to maintain a specimen test temperature of 1200°C under laminar flow conditions. In general, it was necessary to use lower initial power for the unpreoxidized specimens, especially those electropolished, than that used for those specimens which had been preoxidized. During the initial few minutes of testing, it was necessary to continually increase the power to maintain a constant test temperature. Once the metallic surfaces were covered with stable oxide scales with essentially the same surface reflectance and emittance, the power approached to a value common to all of the tests. Specimens were oxidized in the arc-heater for times ranging from 12 s to 10 h. All tests for times longer than 30 min were cyclic tests of 30 min duration followed by cooling before the next run. This procedure was repeated until the desired cumulative exposure time was obtained.

The oxide phases present on the oxidized specimens were identified, *in situ*, using standard X-ray diffraction techniques. Oxide morphology was examined in a scanning electron microscope. Specimens were then sectioned, epoxy mounted, metallographically polished, and vapor deposited with a thin layer of carbon. The microstructure of the oxide cross sections was analyzed using a scanning electron microscope equipped with an energy dispersive X-ray (EDX) analyzer. Electron probe microanalysis was carried out using an ARL electron microprobe operated at 15 kV and 0.05 μ ampere beam current. The carbon layer deposited on the specimen surface helped to eliminate shifting of the electron beam at the metal/oxide interface. The MAGIC computer program developed by Colby[20] was used to correct the raw data.

EXPERIMENTAL RESULTS

The oxides produced on the specimens were identified *in situ* by X-ray diffraction. Three oxide phases, *i.e.*, NiO, Cr_2O_3 and ThO_2, were identified, but $NiCr_2O_4$ spinel was not detected on any of the specimens. The relative X-ray intensities of the oxides and the alloy are listed in Table I. Note that the relative X-ray intensity from the three oxides varies from stage to stage as the dynamic oxidation testing proceeds. It should also be noted that the EP and EP + PO specimens exhibit only the [200] alloy reflection. This indicates that the TD-NiCr alloy has a texture orientation, with its [100] planes parallel to the specimen surface. The MP specimen shows a

Table I. X-Ray Diffraction Data of TD-NiCr After Various Surface Pretreatments and Arc-Jet Exposures

Pretreatment and Arc-Jet Exposure	Alloy Substrate		ThO_2				Cr_2O_3			NiO		
	(111)	(200)	(111)	(200)	(220)	(311)	(012)	(104)	(110)	(111)	(200)	(220)
EP		VS	W	VW	VW	VW						
EP 1 min		VS	W	VW	VW	VW	VW	M	VW	W	S	W
EP 10 min		VS	W	VW	VW	VW	VW	W		W	M	W
EP 2 h		S	M	W	W	W	VW	VW		S	S	S
EP + PO		VS								S	VS	S
EP + PO 30 s		VS								S	VS	S
EP + PO 1 min		VS								S	VS	S
EP + PO 3 min		VS								S	VS	S
EP + PO 10 min		VS	M	W	W		W	W	W	W	M	W
EP + PO 30 min		VS	W			VW	VW	W	W	M	VS	M
EP + PO 2 h		VS	M	M	W	VW	VW	W	W	M	S	W
EP + PO 10 h		VS	S	M	M	M	VW	W	W	M	M	W
MP	W	VS	W	VW	VW	VW						
MP 15 s	M	VS	W	VW	VW	VW	VW					
MP 1 min	M	VS	W	VW	VW	VW				VW	VW	
MP 10 min	M	VS	W	VW	VW	VW	VW	W	W	M	S	M
MP 2 h	VW	S	M	W	W	W	VW	W	VW	M	M	W
MP + PO	M	VS	M	W	W	W	W	M				
MP + PO 15 s	M	VS	W	VW	VW	VW	VW					
MP + PO 1 min	W	VS	W				VW	W		S	S	S
MP + PO 10 min	VW	VS	VW				VW	W	VW	S	VS	S
MP + PO 2 h		VS	M	W	W	W	W	W	VW	M	M	W
MP + PO 10 h		VS	S	M	M	M	W	W	VW	M	M	M

EP = Electropolished
EP + PO = Electropolished and preoxidized
MP = Mechanically polished
MP + PO = Mechanically polished and preoxidized
VS = Very strong; S = strong; M = medium; W = weak; VW = very weak; Blank = not detected.

weak [111] and a very strong [200] reflection. During oxidation, static or dynamic, the [111] reflection intensifies when the specimen is exposed to the high temperature environment. In the static preoxidation, the peak height of the [111] reflection increases by a factor of four after only 15 s of exposure, and reaches a maximum of slightly higher intensity after 1 min of exposure. This intensification of the [111] reflection can be taken as evidence of recrystallization of the deformed surface layer in the early stage of oxidation. The effect of this recrystallization is to promote the selective formation of Cr_2O_3 in a static environment.[12] Its effect on the dynamic oxidation behavior of the alloy will be discussed later in this paper.

The following sections describe each type of surface pretreatment. Scanning electron micrographs showing surface oxide morphology and oxide cross section, EDX patterns indicating oxide chemistry, and electron microprobe scans showing compositional profiles are presented sequentially according to the surface pretreatment.

Electropolished and Preoxidized Surface (EP + PO)

The micrographs and EDX patterns taken of a specimen after 1 h of static oxidation in air at 1100°C are shown in Fig. 1. A compound oxide layer formed on the specimen surface is seen in Fig. 1(*b*). This layer consists of, as identified by the EDX patterns, an external layer of NiO, an intermediate layer of duplex oxide containing both NiO and Cr_2O_3, and a continuous inner layer of Cr_2O_3. The EDX pattern taken of the external NiO at spot-3 shows no sign of thorium peak, indicating that the NiO grew externally by outward diffusion of Ni ions which react with oxygen at the gas/oxide interface. The oxide grains grew predominantly along certain crystallographic directions, thus resulting in a faceted appearance with sharp grain ridges and valleys, see Fig. 1(*a*). The intermediate oxide, composed of Cr_2O_3 particles embedded in porous NiO matrix, appears to be porous and grainy. The fact that a thorium peak is clearly detected in the corresponding EDX pattern (spot-2 pattern) suggests that this oxide layer is produced by internal oxidation. Partial dissociation of NiO must have taken place in this duplex oxide layer to provide Ni and O ions required for the observed external growth of NiO and internal oxidation of the alloy. As a consequence of massive outward flow of Ni ions, the NiO in this duplex oxide layer becomes very porous in nature. Oxygen ions can penetrate readily through this layer for further internal oxidation. The continuous inner oxide layer, Cr_2O_3 (see spot-1 EDX pattern) adjacent to the alloy, is formed by lateral growth of Cr_2O_3 particles at the internal oxidation front. The formation of this oxide layer effectively slows down the progress of internal oxidation. Although multiple oxide layers were observed on the EP + PO specimens, only NiO was detected in the X-ray diffraction studies (Table I). Absorption of the incident and diffracted X-ray beams by the external NiO reduced the intensity diffracted by the inner Cr_2O_3 below the minimum detectable level.

Low magnification micrographs taken of the EP + PO specimens clearly showed the alloy grain structure. Selective oxidation of Cr along the alloy grain boundaries greatly reduced the local external

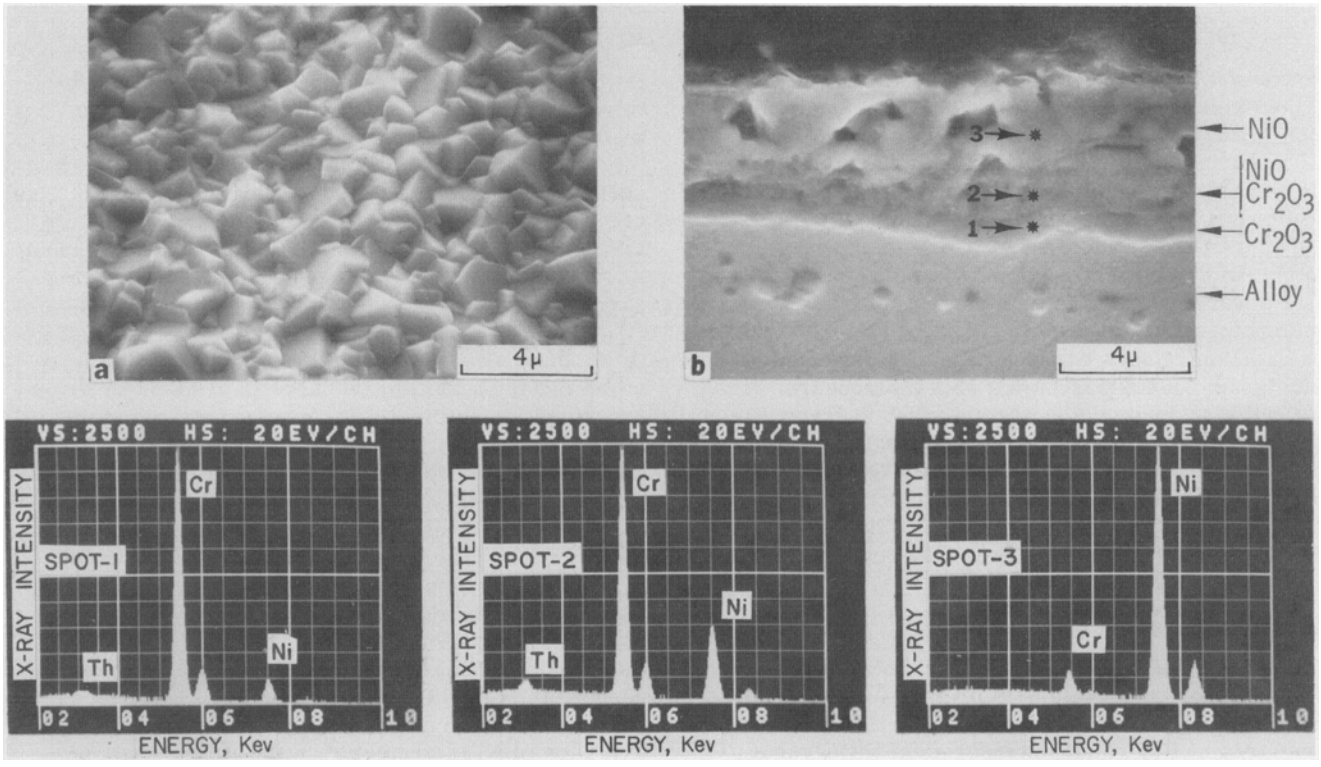

Fig. 1—(*a*) Oxide morphology and (*b*) oxide cross section of electropolished and preoxidized (1 h in static air at 1100°C) specimen. Energy dispersive X-ray analyses were made of the different oxide layers shown in (*b*) indicating variation of Cr, Ni and Th contents.

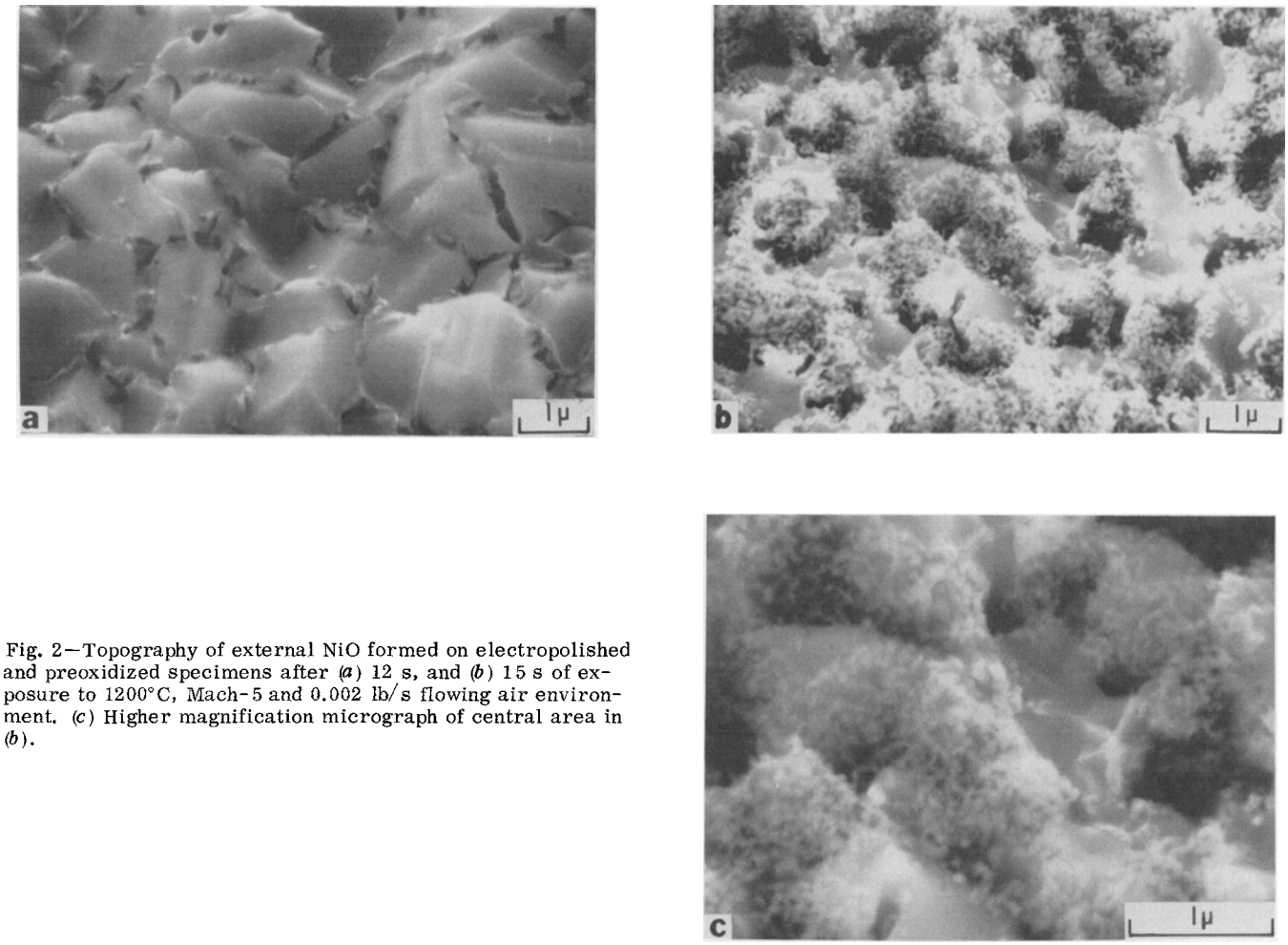

Fig. 2—Topography of external NiO formed on electropolished and preoxidized specimens after (*a*) 12 s, and (*b*) 15 s of exposure to 1200°C, Mach-5 and 0.002 lb/s flowing air environment. (*c*) Higher magnification micrograph of central area in (*b*).

growth of NiO, and therefore caused valleys to appear on the oxidized specimen surface along the original alloy grain boundaries.

The surface oxide morphologies formed on the EP + PO specimens after 12 and 15 s of exposure to the flowing environment are illustrated in Fig. 2. It should be noted that according to measurements made using an optical pyrometer, approximately 10 to 12 s were required to heat a specimen to the test temperature. After 12 s of exposure, Fig. 2(*a*), voids and cracks are seen on the surface, mostly along oxide grain boundaries. After 15 s of exposure, Figs. 2(*b*) and 2(*c*), large voids are observed at lower areas of the surface, mainly at oxide grain valleys. Some porous mass, which is identified as NiO, is seen to condense at higher locations on the surface, predominantly at oxide grain ridges. Obviously, mass transport from oxide grain boundary regions to oxide grain ridges has taken place at the specimen surface immediately upon exposure to the high temperature flowing air.

Grimley *et al*[21] has reported that the vaporization of NiO at high temperature is predominantly by dissociation of NiO into its elements. Equilibrium partial pressures of Ni(v) and O measured on NiO(s) under neutral conditions were reported to be two orders of magnitude greater than that of NiO(v). It will be shown later (Fig. 5) that the oxide morphologies illustrated in Fig. 2 may be observed only if specimens are tested in a gas stream containing oxygen. It is therefore proposed that the observed mass transport phenomenon develops following three processes. They are: 1) vaporization of NiO at oxide grain boundary areas mainly by dissociation of NiO into Ni(v) and O, 2) reoxidation of Ni vapor, presumably with atomic oxygen in gas stream, and 3) condensation of NiO at raised points on the surface. The stagnation layer under the present test conditions was reported to be of the order of 360 μm.[22] There is gradient in oxygen concentration and in total pressure across the thickness of the stagnation layer. Vaporization of NiO appears to proceed at a faster rate at areas lower than the average specimen surface level where the oxygen partial pressure is lower under the flowing conditions. Consequently, voids and cracks are observed mostly along oxide grain valleys. Reoxidation of Ni vapor tends to take place at a greater rate at locations above the average surface level where the oxygen partial pressure is higher. Therefore, condensation of NiO occurs mostly at higher locations on the specimen surface where the rate of reoxidation of Ni is greater than the rate of dissociative vaporization of NiO.

During subsequent oxidation, the vaporization-con-

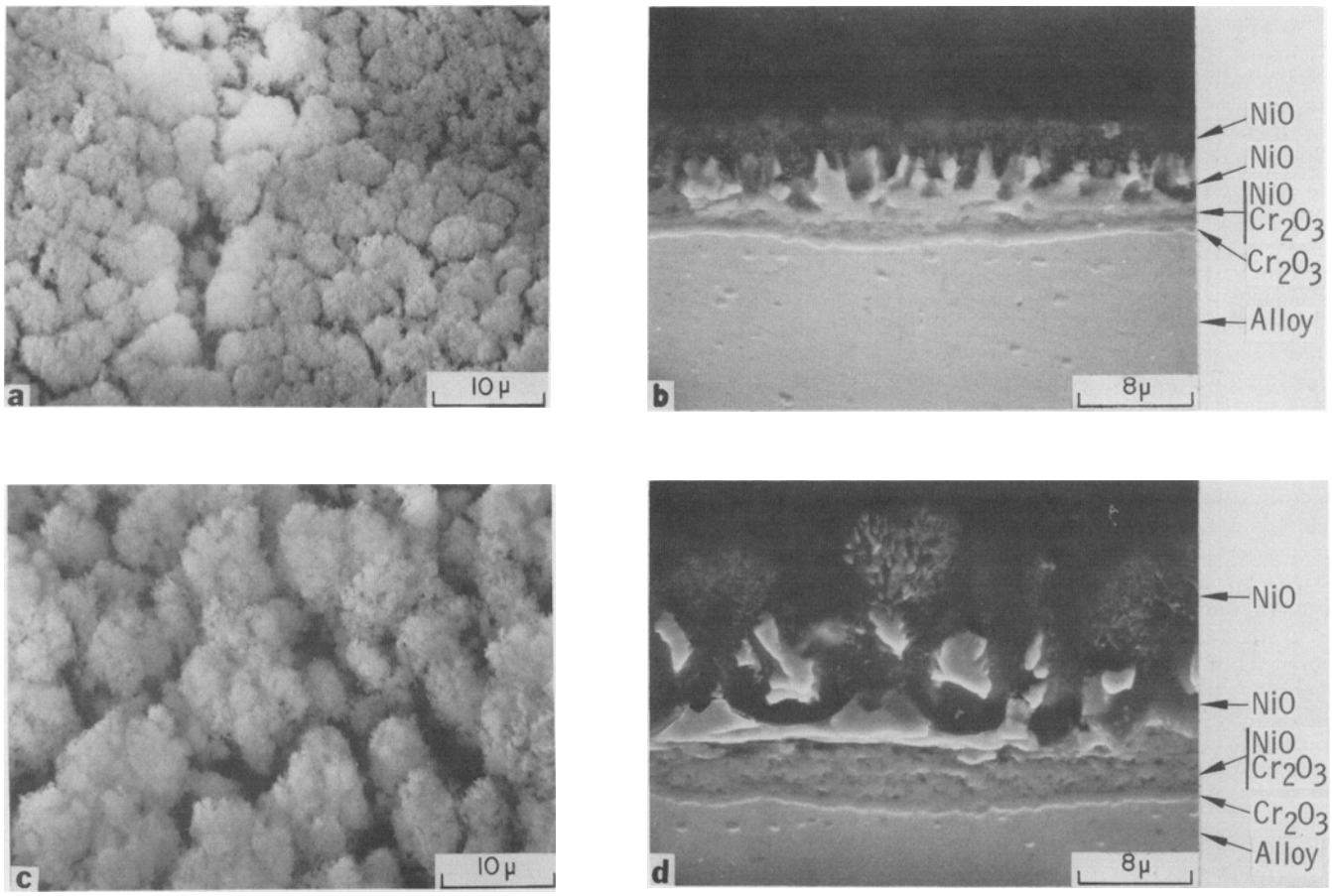

Fig. 3—Surface morphology and oxide cross sections of electropolished and preoxidized specimens after (*a*), (*b*) 1 min, and (*c*), (*d*) 10 min of dynamic oxidation.

densation process brings about some drastic changes in the oxide morphology. At 1 min of oxidation, the specimen surface is covered with a layer of very porous oxide, see Fig. 3(*a*). High magnification photographs and EDX patterns reveal that the porous oxide consists of numerous fine NiO crystals, with an appearance similar to that sometimes observed for crystals growing under condensation processes. The oxide cross section of the same specimen is shown in Fig. 3(*b*). The top portion of the original NiO, which formed during static preoxidation, degrades as a result of vaporization. Fine particles of NiO are growing on top of the degraded NiO layer as a consequence of condensation of reoxidized NiO. The oxides underneath the degraded layer remain essentially uneffected.

After 10 min of oxidation, most of the specimen surface is covered with a layer of NiO with a mushroom-type or "cotton ball"-type morphology, see Fig. 3(*c*). NiO mushroom clusters smaller than those shown in the figure were observed at other areas, predominantly the areas near alloy grain boundaries. The microstructure of the oxide cross section at areas where large mushrooms developed is given in Fig. 3(*d*). The NiO clusters consisting of fine NiO particles are supported by oxide stems which are the remains of the original NiO. The mushroom oxide grows at the expense of the original NiO layer. Although part of the NiO condenses on growing mushrooms, a significant fraction of the NiO is carried away by the flowing gas. Most of the original NiO disappears after about 1.5 h of oxidation. From this stage on the existance of mushroom oxide depends on the NiO in the duplex oxide layer. As the NiO content in the duplex oxide layer is lowered (see spot-2 pattern in Fig. 1), the mushroom clusters start to reduce in size because the rate of condensation of NiO becomes less than the rate of loss to the air stream.

Micrographs taken of a specimen with 2 h of exposure are presented in Fig. 4. These micrographs are also typical for specimens after 10 h of oxidation. At this later stage of oxidation, most of the specimen surface is covered with small NiO clusters, which have a relatively smooth surface appearance compared with that of the large mushrooms found in the earlier stages of oxidation. A typical micrograph showing these small mushroom-type clusters is given in Fig. 4(*a*), and a micrograph revealing the corresponding oxide cross section is presented in Fig. 4(*b*). There are some areas on the specimen surface where the duplex oxide totally disappears. The inner Cr_2O_3 layer is subject to rapid vaporization, and the alloy is exposed directly to the flowing air. Microprobe analysis made at these areas generally shows extensive Cr depletion in the alloy, mostly 10 to 15 pct at the alloy/oxide interface. There are also other regions on the specimen surface where local internal oxidation is clearly observed. An example is given in Fig. 4(*c*). Results of a probe scan made along the marked line shown in Fig. 4(*c*) are presented in Fig.

4(*d*). The Cr content in the alloy at the interface is found to be approximately 15 pct. Pile-up of ThO_2 particles at the outer portion of the duplex oxide layer is frequently observed. In addition to the two types of oxide cross sections described above, there are other regions where large NiO mushrooms are seen to grow on top of solid NiO, and under the solid NiO, internal oxidation is invariably detected.

To further enlighten the mechanism proposed for the formation of mushroom-type oxide, tests were conducted on the EP + PO specimens in Mach-5 flowing N_2 at 1200°C for times ranging from 15 s to 1 h. The objective was to determine the changes in surface oxide morphology resulting from high speed gas flow over the specimen where little or no oxygen was present. X-ray diffraction patterns taken of the exposed specimens showed only NiO and Cr_2O_3 reflections. There were no nickel or chromium nitride phases detected. Typical micrographs of the exposed specimens are shown in Fig. 5. After 15 s of exposure, Fig. 5(*a*), there is a rounding of the sharp NiO grain ridges, and a development of cavities at the oxide grain boundary regions. After 10 min of exposure there is an increase in the NiO grain size, and a further opening up of the cavities in the NiO layer, see Fig. 5(*b*). As the test proceeds, the NiO layer at the alloy grain boundaries disappears by virtue of vaporization. The exposed alloy grain boundary regions which are still covered with Cr_2O_3 are clearly visible (the dark areas) in Fig. 5(*c*). The Cr_2O_3 oxide phase is stable in the N_2 environment because the formation of volatile CrO_3 is prevented due to the absence of oxygen. The surface NiO disappears totally from the specimen surface after about 1 h of exposure. The above observations demonstrate that the presence of oxygen is necessary for the redeposition of NiO and the subsequent growth of mushroom-type oxide.

Mechanically Polished and Preoxidized Surface (MP + PO)

The static oxidation behavior of the MP specimens was also studied. After 1 h of oxidation in air at 1100°C, the specimen surface was covered with a layer of globular Cr_2O_3 approximately 1 to 2 μm thick, see Fig. 6.

When MP + PO specimens were exposed to the dynamic environment, the external Cr_2O_3 was further oxidized to form volatile CrO_3. Results of X-ray diffraction analysis indicate that the external Cr_2O_3 almost disappears from the specimen surface after 15 s of exposure, and subsequently a NiO layer grows rapidly on the specimen surface.

At 1 min of exposure, the specimen surface was

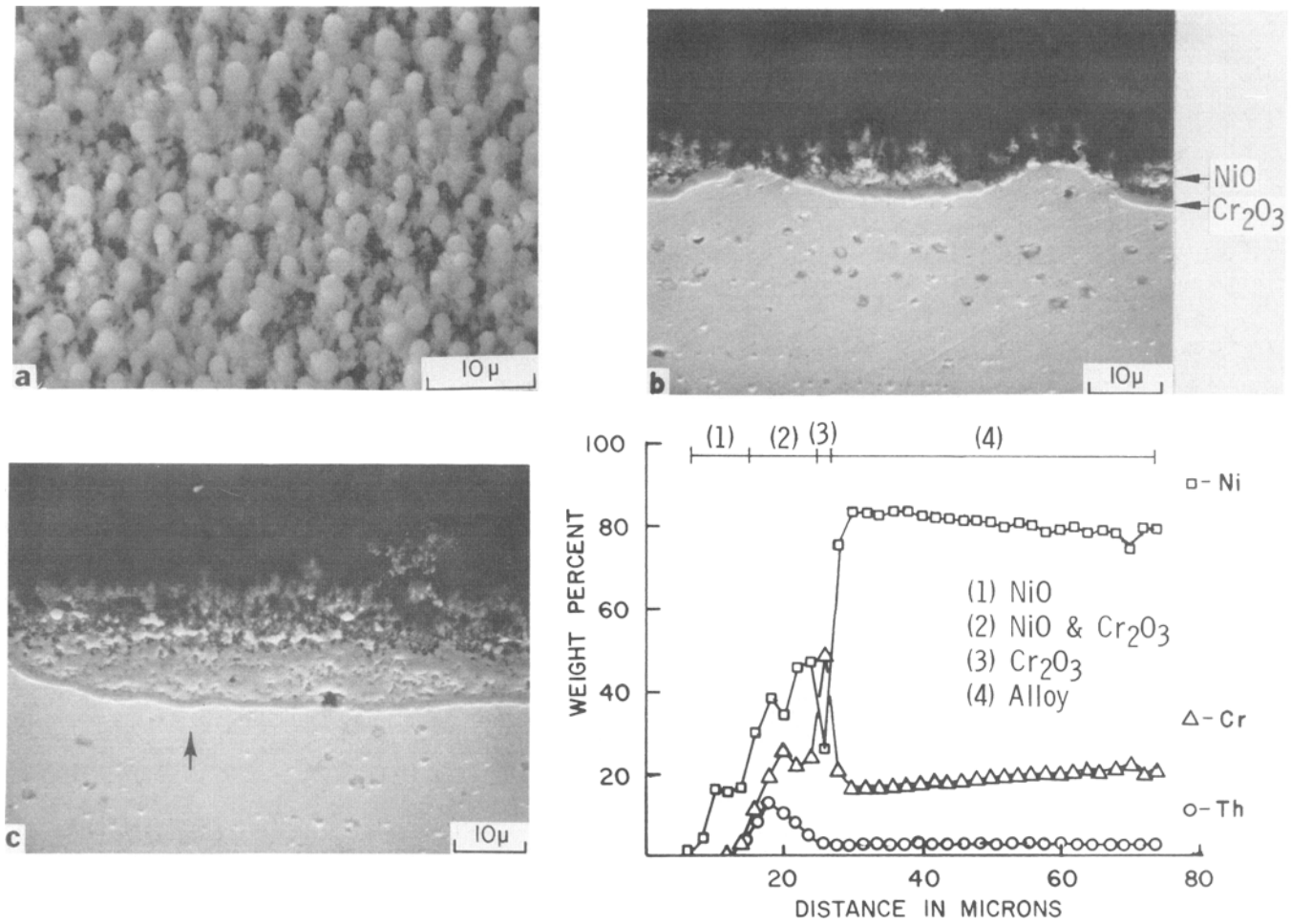

Fig. 4—Typical oxide topography and oxide cross sections observed on electropolished and preoxidized specimen after 2 h of exposure to the dynamic environment. Probe scan was made along the line marked with an arrow in (*c*).

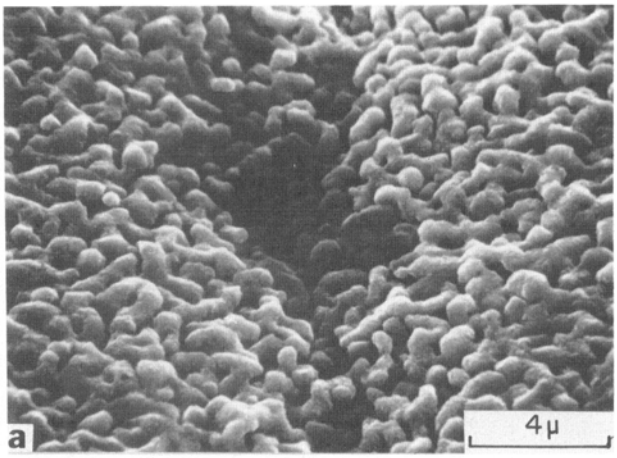

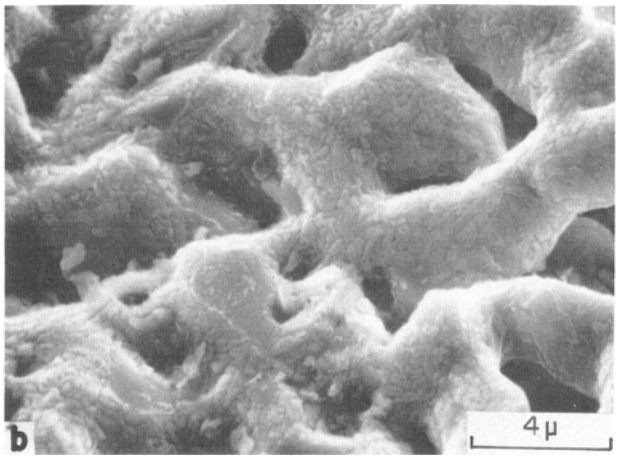

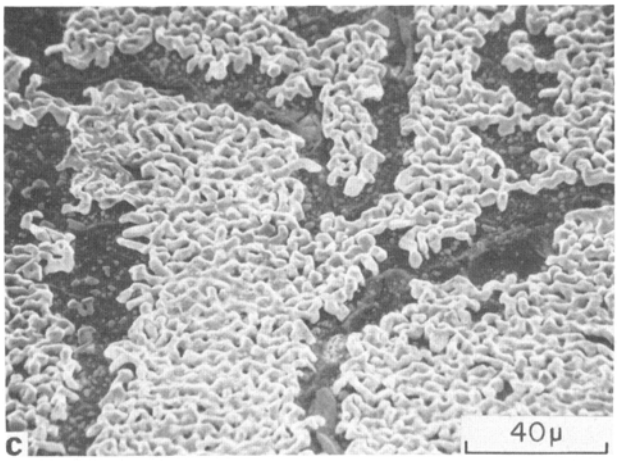

Fig. 5—Surface topography of electropolished and preoxidized specimen after (*a*) 15 s, and (*b*) 10 min of exposure to a Mach-5, 1200°C and 0.002 lb/s flowing N_2 gas. (*c*) A lower magnification micrograph of 10 min exposure specimen.

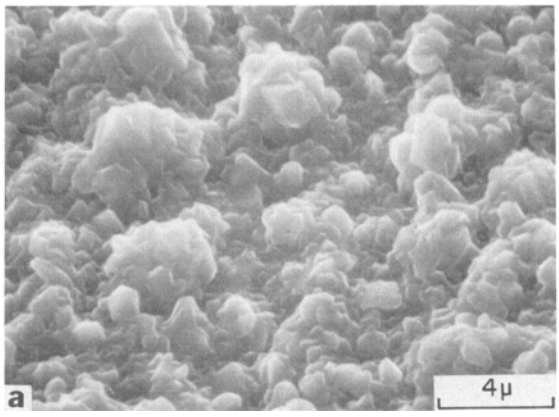

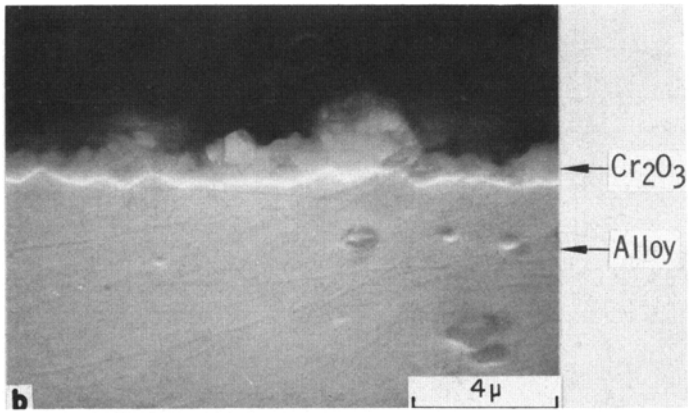

Fig. 6—Morphology of external Cr_2O_3 and oxide cross section of mechanically polished and preoxidized (1 h in static air at 1100°C) specimen.

covered with a porous mushroom-type NiO oxide, see Fig. 7(*a*). The cross-sectional micrograph, Fig. 7(*b*), shows that the mushroom oxide grows on top of a relatively solid NiO layer which is formed by external growth. Under the NiO layer a duplex oxide resulting from internal oxidation is observed. At this stage of oxidation, no inner Cr_2O_3 layer has yet formed at the oxide/alloy interface. As oxidation proceeds, a continuous Cr_2O_3 layer eventually develops and internal oxidation effectively stops. Mushroom oxide clusters continue to grow at the expense of the underlying NiO. After 10 min of exposure, Fig. 7(*c*) and 7(*d*), oxidation proceeds in the same sequence as that previously presented for the EP + PO specimens.

The MP + PO specimens were also tested in a flowing N_2 environment. At 15 s of exposure no changes were detected in Cr_2O_3 morphology. After 10 min of exposure, changes in oxide topology were observed. A typical micrograph is shown in Fig. 8(*a*). X-ray diffraction analysis indicated that the surface

layer shown in the photograph is Cr_2O_3. The Cr_2O_3 appears in the shape of mushroom-type morphology with small solid pillars protruding from the alloy substrate. Careful comparison of the photographs taken before and after the N_2 exposure suggests that the small pillars observed in Fig. 8(*a*) are the remains of the original large Cr_2O_3 globules. Apparently, vaporization of Cr_2O_3 occurs under the neutral flowing conditions. According to Grimley *et al*,[23] vaporization of Cr_2O_3 under neutral conditions proceeds with the formation of Cr, CrO, CrO_2, O and O_2 as the principal gaseous species.

After a 10 min N_2 exposure, the MP + PO specimens were then oxidized in flowing air conditions. Immediately upon exposure, a sudden glow at the shock wave was detected, presumably the result of rapid vaporization of the Cr_2O_3 pillars. A typical micrograph taken from the 10 min N_2 exposure specimen after an addi-

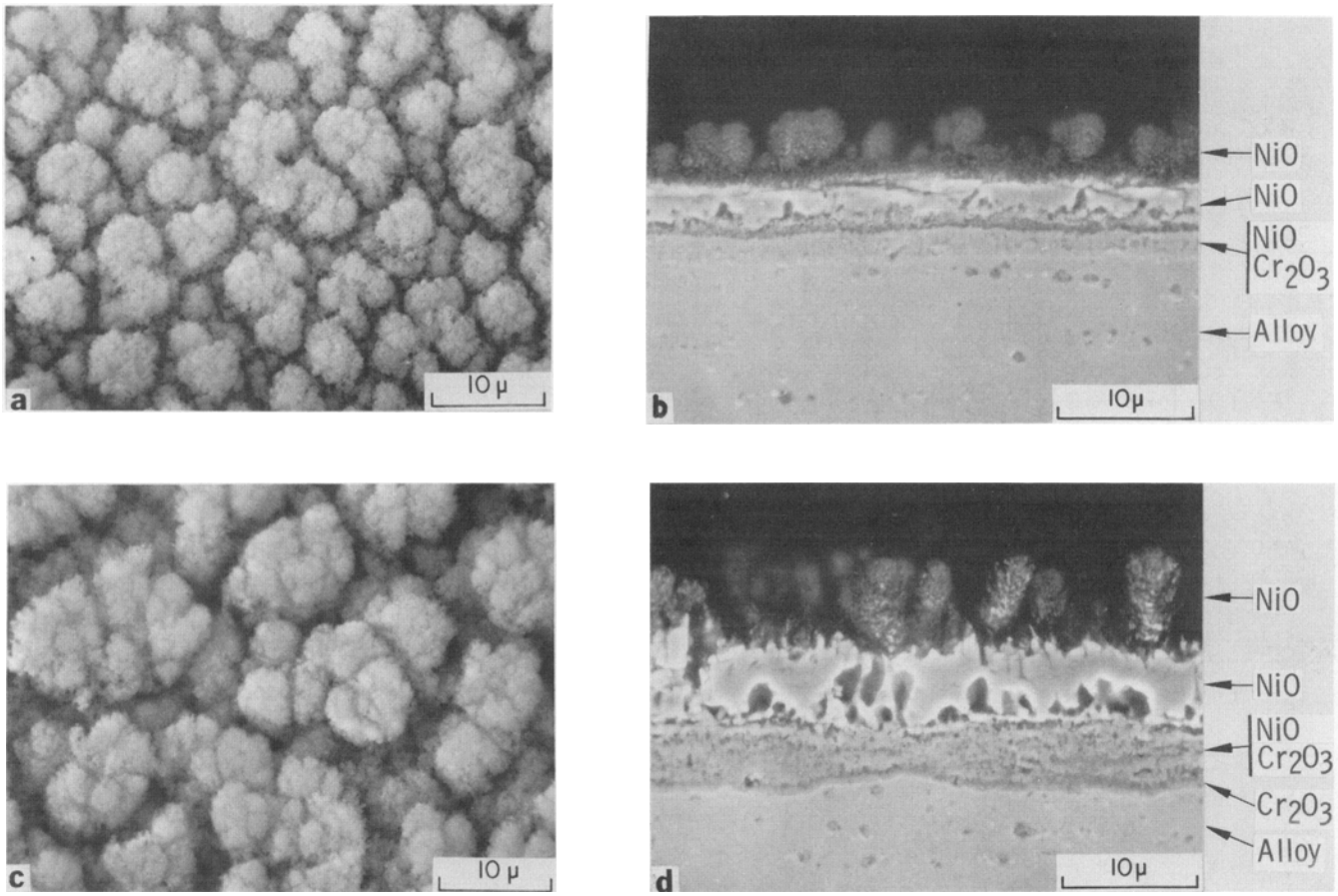

Fig. 7—Oxide topography and cross sections of mechanically polished and preoxidized specimens after (*a*), (*b*) 1 min, and (*c*), (*d*) 10 min of dynamic oxidation.

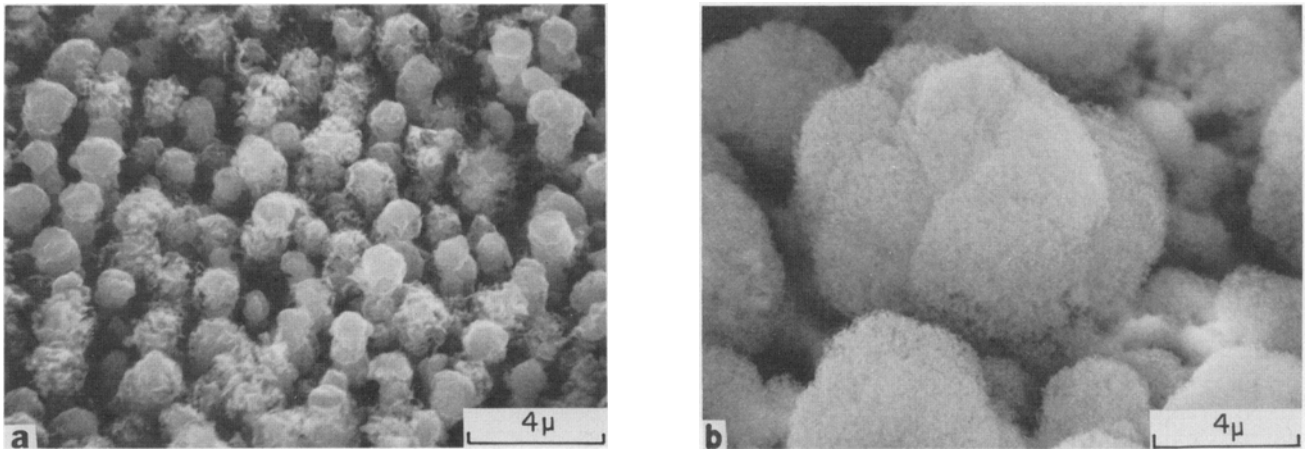

Fig. 8—Surface morphology of mechanically polished and preoxidized specimen after (*a*) 10 min of exposure to flowing N_2 gas, and (*b*) subsequent 5 min exposure to flowing air environment.

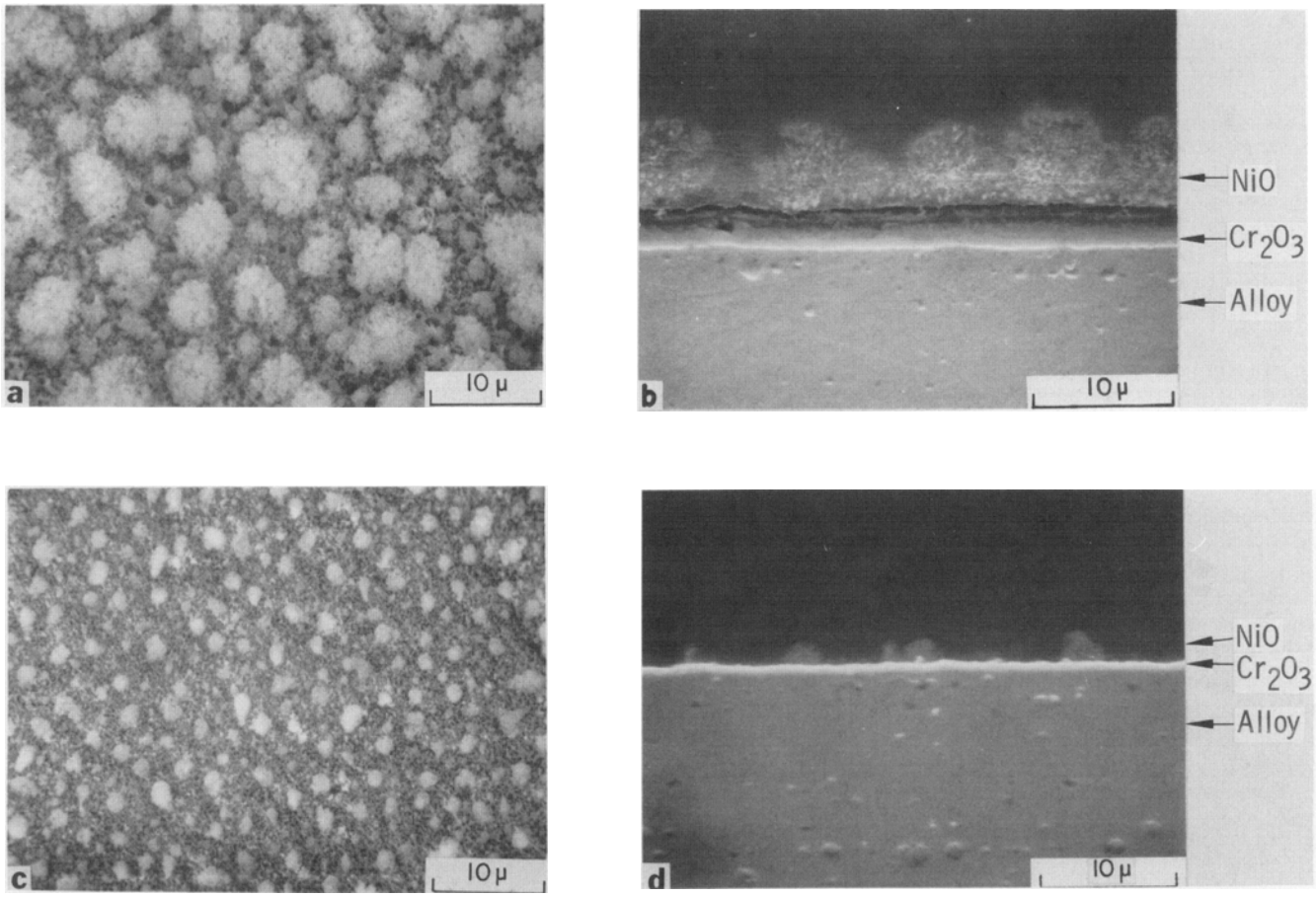

Fig. 9—Oxide topography and cross sections of electropolished specimens after (*a*), (*b*) 1 min, and (*c*), (*d*) 10 min of dynamic oxidation.

tional 5 min of air exposure is shown in Fig. 8(*b*). The surface is uniformly covered with NiO clusters typical of the type of morphology found for short time air tests.

Electropolished Surface (EP)

Figs. 9(*a*) and 9(*b*) show the micrographs taken of an EP specimen after 1 min of oxidation. The entire surface, with the exception of the alloy grain boundary areas, is covered with mushroom-type oxide clusters. A uniform and continuous Cr_2O_3 layer is seen underneath the mushroom NiO. Although porous, the NiO mushrooms do serve to protect the Cr_2O_3 from oxidative vaporization. No internal oxidation is yet observed at this stage. As the oxidative process proceeds, both the number and size of the NiO mushrooms decrease, and the Cr_2O_3 layer becomes thinner. This is seen in Figs. 9(*c*) and 9(*d*) which are photographs taken of a 10-min exposure specimen. Apparently, the porous NiO is still protecting the underlying Cr_2O_3. However, at some areas on the specimen surface, islands of large NiO mushrooms were observed, and internal oxidation was always found under these areas. After 2 h of exposure, the specimen surface was entirely covered with large oxide clusters. The oxide morphology and cross section were very similar to those observed on the EP + PO specimens after approximately 10 min of oxidation. It is apparent that the initial oxidation rate of the EP specimen is slower than those of the EP + PO and MP + PO specimens.

Mechanically Polished Surface (MP)

Figs. 10(*a*) and 10(*b*) demonstrate the typical oxide structure of an MP specimen after 1 min of oxidation. Scattered islands of NiO mushrooms are seen to grow on the specimen surface. Under these mushroom islands, concurrence of external growth of NiO and internal oxidation of the alloy is detected. Away from the islands, small NiO clusters are seen to grow on ridges of the surface scratches caused by mechanical polishing. Under these small oxide clusters a thin layer of Cr_2O_3 is generally observed. During subsequent oxidation the mushroom clusters increase in size, and the mushroom islands spread to cover the whole surface. This is illustrated in the micrographs shown in Figs. 10(*c*) and 10(*d*) which represent the typical oxide structure of a specimen after 10 min of exposure. The specimen surface is essentially covered with large NiO mushrooms. There are small regions where small mushrooms are still growing on top of a thin Cr_2O_3 layer. At 2 h of oxidation the oxide structure is similar to that observed on the EP + PO specimens with the same exposure.

DISCUSSION

From the above observations it is evident that in spite of the difference in surface pretreatment, the external oxide developed under the Mach-5 and 1200°C flowing air conditions is a layer of porous NiO in the mushroom-type morphology. The development of this mushroom oxide can be accounted for by the proposed vaporization-reoxidation-condensation processes. Vaporization of NiO proceeds predominantly by dissociation into its elements, *i.e.*,

$$NiO(s) = Ni(v) + O.$$

A decrease in partial pressure of either Ni(v) or O, or both, favors the dissociative vaporization, whereas the reverse enhances the oxidation process forming the solid oxide phase. There is a gradient of oxygen partial pressure across the stagnation layer on the specimen surface. Vaporization of NiO therefore occurs at low regions on the surface where the oxygen partial pressure is low, and reoxidation of the dissociated Ni atoms proceeds at high regions on the surface where the oxygen concentration is higher. Part of the oxidized NiO molecules are constantly carried away by the flowing gas stream, and part of them condense on the elevated sites of the specimen surface resulting in the formation of porous mushroom oxide.

The formation of mushroom oxide requires the presence of oxygen in the flowing gas condition. This was clearly demonstrated in the flowing N_2 test where no oxygen was introduced in the gas stream, and only vaporization of NiO was observed. The development of mushroom oxide also requires high partial pressure of Ni(v). This was evident from the observations that mushroom clusters grew in size on a solid NiO layer, and faded when the underlying NiO was consumed.

The introduction of oxygen into the flowing gas stream slightly reduces the vaporization rate of NiO, and greatly increases the vaporization rate of Cr_2O_3. The external NiO layer, 3 μm thick, formed on the EP + PO specimen was found to disappear after about 1 h of exposure to the N_2 test. With the presence of oxygen which caused condensation of some reoxidized NiO, the same external NiO was found to disappear after about 1.5 h of exposure. The latter observation corresponds to a vaporization rate of approximately 3.6×10^{-7} gm/cm^2/s. The external Cr_2O_3 layer, 1 μm thick, produced on the MP + PO sample was still in contact with the metal substrate after a 10 min N_2 exposure. With the introduction of oxygen, however, the same oxide was found to nearly disappear after 15 s of testing. This observation indicates a Cr_2O_3 vaporization rate of approximately 1×10^{-4} gm/cm^2/s; the compensated exposure time at 1200°C was taken to be 5 s, since the time needed to reach the test temperature was about 12 s. The loss rate of Cr_2O_3 is more than two orders of magnitude greater

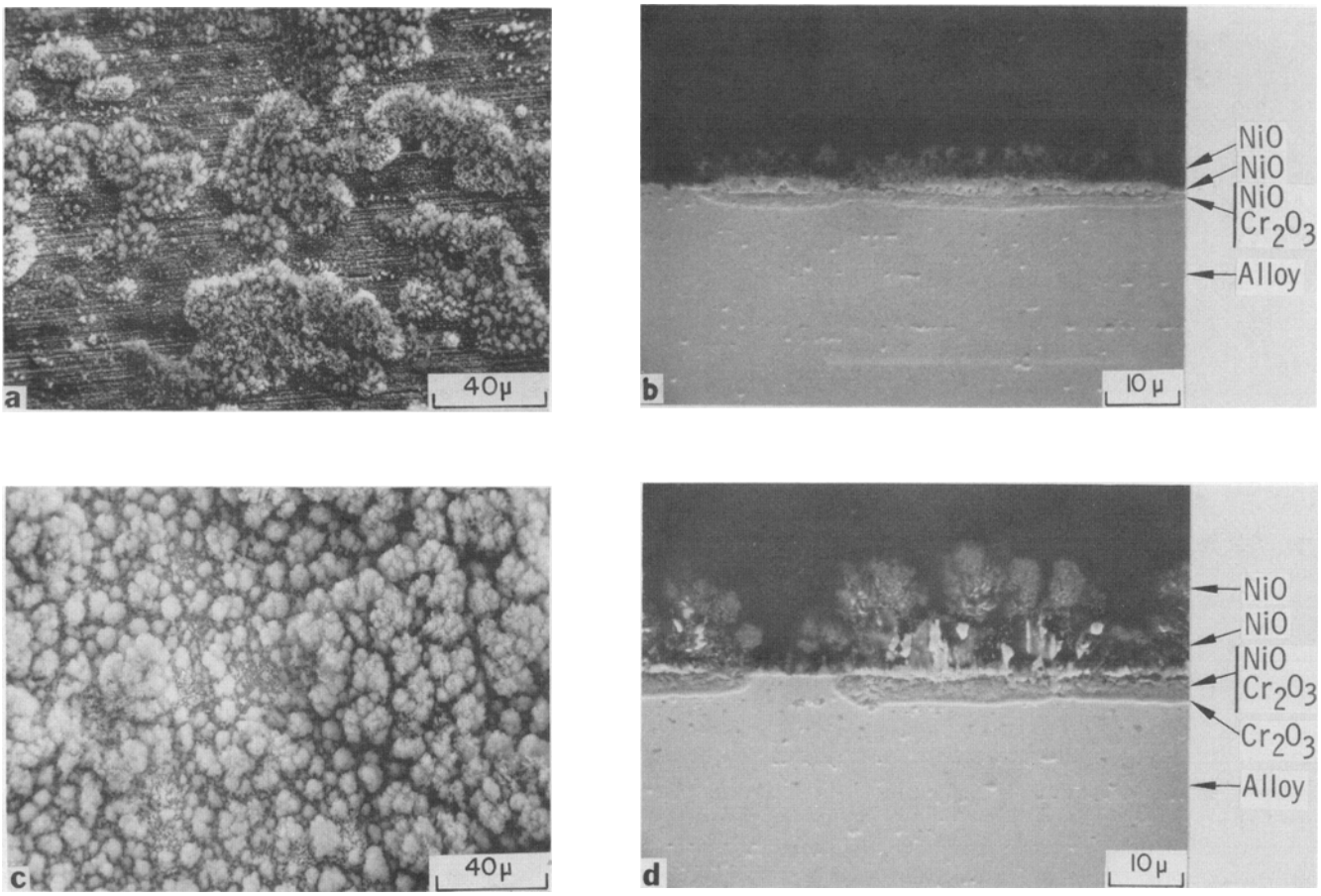

Fig. 10—Oxide morphology and cross sections of mechanically polished specimens after (*a*), (*b*) 1 min, and (*c*), (*d*) 10 min of dynamic oxidation.

than that of NiO. Therefore it can be concluded that the loss rate of NiO in the vaporization and condensation processes is the rate controlling factor in the present dynamic oxidative condition. The rapid vaporization rate of Cr_2O_3 is attributed to the presence of atomic oxygen in the air stream which greatly enhances the formation of volatile CrO_3.

Surface pretreatment has a significant effect on the static oxidation behavior of the TD-NiCr alloy. Mechanical polishing causes a deformed surface layer which undergoes recrystallization upon exposure to the high temperature environment, and a fine-grain layer forms on the specimen surface. The recrystallized surface layer provides numerous preferential sites, the grain boundary areas, for selective formation of Cr_2O_3, which grows to cover the whole specimen surface. Removal of the surface deformation layer by electropolishing leads to the formation of a compound oxide consisting of an external layer of NiO, and intermediate layer of NiO and Cr_2O_3 mixture, and an inner layer of Cr_2O_3. The NiO, although not as thermodynamically favored as Cr_2O_3, forms faster than Cr_2O_3 on grain surfaces and then grows laterally to cover the grain boundary areas where Cr_2O_3 selectively forms.

Surface pretreatment also has a significant effect on the dynamic oxidation behavior of TD-NiCr, particularly in the early stage of oxidation. The EP + PO treatment produces a solid external NiO which changes to the mushroom oxide morphology under high speed flowing air condition. Details of the oxidation process have been described in the results section.

The MP + PO treatment results in an external Cr_2O_3 surface scale on a recrystallized alloy surface layer. Upon exposure to the air stream the Cr_2O_3 layer immediately evaporates exposing the chromium depleted alloy directly to the air stream. A layer of NiO subsequently forms on the surface and is converted to a mushroom type morphology. Since this layer is porous, oxygen can readily penetrate to the alloy substrate resulting in internal oxidation of both nickel and chromium. The numerous grain boundaries in the recrystallized alloy surface layer tend to enhance internal oxidation of the alloy. The grain boundary regions near the surface tend to be opened up as a result of vaporization of Cr_2O_3 initially present from the PO treatment. Any NiO which forms following the loss of the Cr_2O_3 will dissociate more rapidly at the boundary areas than at more elevated locations on the surface, such as centers of grains. Both the vaporization of Cr_2O_3 and dissociation of NiO at the boundary regions tends to open up the boundaries making them paths for rapid mass transport of oxygen into the alloy and nickel out. Undoubtedly the processes involved include vapor transport, surface, and grain boundary diffusion.

The rapid and massive outward flow on Ni ions leaves behind a porous zone filled with vacancies which greatly enhances internal oxidation of both nickel and chromium and delays the development of a continuous inner Cr_2O_3 layer. When the inward penetration slows down at the nonrecrystallized region, an inner layer of Cr_2O_3 forms at the oxidation front. When this layer becomes continuous and coherent it effectively stops internal oxidation of the alloy by blocking the inward diffusion of oxygen and the outward diffusion of nickel. This oxidation chronology is clearly evident in the micrographs shown in Fig. 7 and the X-ray results given in Table I. At 1 min of oxidation, an internally oxidized layer is found without an inner layer of Cr_2O_3 and the (111) reflection from the alloy is still measurable. At 10 min of oxidation, an inner Cr_2O_3 is observed, and the alloy (111) line is very weak.

The above observations suggest that the depth of internal oxidation of the MP + PO sample at the early stage of oxidation is dependent on the depth of surface deformation caused by mechanical polishing. The original purpose of the MP + PO treatment was to produce a layer of external Cr_2O_3 which had a high surface reflectance and emittance for improved oxidation resistance to the dynamic environment. The results of this investigation however suggest that the pretreatment enhances rather than decreases metal recession during the early stages of oxidation.

The MP treatment produces a surface deformation layer which undergoes recrystallization upon exposure of the specimen to the high temperature dynamic oxidation environment. Since recrystallization is a thermally activated process it proceeds nonuniformly at the deformed surface layer, fast rates of oxide growth at recrystallized regions results in the formation of NiO mushroom islands on the specimen surface at 1 min of exposure, see Fig. 9(*b*). During subsequent oxidation recrystallization of the surface layer proceeds and mushrooms spread to cover the entire surface.

The EP treatment removes the deformed surface layer. Upon exposure to the dynamic environment an external layer of NiO forms on the surface which then converts to the mushroom-type morphology. Underneath the NiO a continuous Cr_2O_3 layer forms at the metal/oxide interface. Although porous, the NiO does protect the underlying Cr_2O_3 from rapid vaporization. As the oxidation process proceeds, both the number and size of NiO mushroom clusters decrease, and the Cr_2O_3 layer becomes thinner. The surface and cross-section of a 10 min exposure specimen are shown in Figs. 9(*c*) and 9(*d*). With increasing exposure time the Cr_2O_3 layer will continue to reduce in thickness due to the combined effects of a faster rate of Cr_2O_3 vaporization attributed to the loss of protecting NiO and a slower rate of growth of Cr_2O_3 due to chromium depletion of the underlying alloy. As oxidation proceeds a point will be reached where the Cr_2O_3 layer is lost exposing the alloy directly to the environment. This gives rise to external growth of NiO mushrooms with accompanying internal oxidation of the alloy. It was generally observed that internal oxidation proceeded into the chromium depleted alloy until a depth was reached where the chromium content was approximately 15 pct. This seemed to be the Cr content needed for the development of a continuous inner Cr_2O_3 layer at the metal/oxide interface.

At the later stage of oxidation when the pretreatment effect is washed out, the oxidation of the alloy is characterized by a cyclic process which occurs to a different stage at different regions on the specimen surface. At regions where the duplex oxide is con-

sumed, the inner Cr_2O_3 quickly vaporizes, thus exposing the Cr-depleted substrate (generally to about 10 pct Cr) directly to the oxidizing atmosphere. This is followed by simultaneous processes of external growth of solid NiO and internal oxidation of the alloy. The internal oxidation halts when a layer of inner Cr_2O_3 forms, with the depth of penetration dependent on the extent of Cr depletion at the localized regions. Mushroom oxide grows atop the solid NiO, and fades when the solid NiO vaporized. When the mushroom oxide and the duplex oxide are consumed, a new oxidation cycle emerges. The overall oxidation rate of the alloy is dependent on the rate of vaporization of NiO during the cyclic process and to a lesser extent on the rate of formation of Cr_2O_3 at the metal/oxide interface.

Finally, it should be pointed out that the dynamic atmosphere of Mach-5, 1200°C and 0.002 lb/s flowing air conditions was selected in this investigation to simulate the environment encountered in the crucial part of space shuttle reentry where the thermal protection shield, for which TD-NiCr alloy is considered a candidate material, will experience a temperature maximum of 1200°C. A large fraction of the boundary layer oxygen will be dissociated into atomic oxygen by the shockwave. The fraction of the dissociated oxygen ranges from 0 to 100 pct, depending on altitude and angles of entry attack.[13,14] Under the arc-jet conditions employed in this study, the concentration of atomic oxygen at the specimen surface was reported to be approximately 0.5 pct.[22] Electrical arcing in the arc chamber may produce additional oxygen atoms. Although arc-jets produce an environment high in ionized gases and low in atomic oxygen relative to those encountered in reentry, they do provide a better reentry simulation than any other facility available. The dissociated oxygen, although low in concentration, may impose significant variation in oxidation kinetics of metals. Dickens *et al*[24] indicates that the introduction of 0.02 pct atomic oxygen in an oxidizing atmosphere at 710°C increases the oxidation rate of pure Ni by a factor of fourteen over that observed in molecular oxygen. Fryburg *et al*[25] shows an enhancement of oxidative vaporization of Cr_2O_3 by a factor of 10^9 at 550°C in oxygen containing 2.5 pct atomic oxygen and an enhancement of vaporization of bare Cr by a factor one-half that of Cr_2O_3 at temperatures below 800°C. Gilbreath[13,14] has demonstrated the accelerated oxidation of space shuttle TPS metals in flowing air (12 m/s) which contained a significant amount of atomic oxygen. Metal recession rate is about two orders of magnitude greater in atomic oxygen than in molecular oxygen. In static or flowing O_2, a dark-grey and adhesive surface scale rich in Cr was detected. In flowing O, a yellow-green and friable scale rich in Ni was observed. The external mushroom-type NiO formed during the present dynamic testing is invariably yellowish to greenish white. The mushroom oxide was very friable and a sharp tap or slight bending of the specimen caused much of the oxide to spall. The similarity of visual appearance and oxide identity observed in atomic oxygen and in arc-jet suggests that the dissociated oxygen in the arc-jet air stream plays the most important role in the development of mushroom-type oxide morphology.

CONCLUSIONS

Based on the observations described herein, together with the results reported in the literature, the following conclusions can be made.

1) Under the arc-jet environment, the atomic oxygen in the air stream plays the most important role in determining the oxidation characteristics of TD-NiCr alloy.

2) The high oxidative vaporization rate of Cr_2O_3 makes the Cr_2O_3 a nonprotective oxide in the arc-jet atmosphere.

3) The external oxide found in an environment containing atomic oxygen is a layer of porous NiO in the mushroom-type morphology. Its development follows three steps: a) vaporization of NiO predominantly by dissociation into Ni vapor and O atoms, b) reoxidation of Ni vapor primarily with the dissociated oxygen in air stream, and c) condensation of NiO at elevated sites on specimen surface. The NiO mushrooms grow at the expense of underlying NiO, and fade when the supply for Ni is limited.

4) Surface pretreatment has a significant influence on the oxidation behavior of TD-NiCr alloy. Mechanical polishing induces surface recrystallization in the very early stage of oxidation. In static environment, the recrystallized surface enhances the formation of external Cr_2O_3. In dynamic atmosphere, the recrystallized layer promotes the concurrence of external growth of NiO and internal oxidation of the alloy, and thereby increases initial metal recession rate. Removal of the surface deformation layer by electropolishing slows down the initial oxidation rate.

5) At the later stage of oxidation when the effect of surface pretreatment is washed out, the oxidation process is characterized by localized oxidation following a cyclic process; each cycle consists of 1) vaporization of fading NiO mushrooms and oxide mixture, 2) rapid vaporization of Cr_2O_3 layer, and 3) concurrence of external growth of NiO and internal oxidation of Cr-depleted substrate. The internal oxidation proceeds to a depth where the formation of an inner Cr_2O_3 becomes favorable. The Cr content at the oxide/metal interface for favorable formation of inner Cr_2O_3 layer appears to be approximately 15 pct.

6) The oxidation rate of the alloy in the arc-jet environment is determined by the rate of loss of NiO during the vaporization-condensation processes.

ACKNOWLEDGMENT

The authors are grateful to the National Aeronautics and Space Administration, Langley Research Center, Hampton, Virginia, for their support of this research.

REFERENCES

1. B. A. Wilcox and A. H. Clauer: *Metal Sci. J.*, 1969, vol. 3, pp. 26-33.
2. B. A. Wilcox, A. H. Clauer and W. S. McCain: *Trans. TMS-AIME*, 1969, vol. 293, pp. 1791-95.
3. B. A. Wilcox and A. H. Clauer: NASA CR-2025, 1972.
4. K. H. Holko: NASA TM-X-52952, 1971.
5. W. A. Sanders and C. A. Barret: NASA TM-X-67864, 1971.
6. G. R. Wallwork and A. Z. Hed: *Oxidation of Metals*, 1971, vol. 3, no. 3, pp. 229-41.

7. J. Stringer, B. A. Wilcox and R. I. Jaffee: *Oxidation of Metals,* 1972, vol. 5, no. 1, pp. 11-47.
8. C. S. Giggins and F. S. Pettit: *Met. Trans.,* 1971, vol. 2, pp. 1071-78.
9. H. H. Davis, H. C. Graham, and I. A. Kvernes: *Oxidation of Metals,* vol. 3, no. 5, pp. 431-51, 1971.
10. C. E. Lowell, D. L. Deadmore, S. J. Grisaffe, and T. L. Drell: NASA TN-D-6290, 1971.
11. C. S. Giggins and F. S. Pettit: *Trans. TMS-AIME,* 1969, vol. 245, pp. 2495-2507.
12. C. S. Giggins and F. S. Pettit: *Trans. TMS-AIME,* 1969, vol. 245, pp. 2509-14.
13. W. P. Gilbreath: NASA TM-X-62064, 1971.
14. W. P. Gilbreath: *Progr. Astronaut. Aeronaut.,* 1972, vol. 31, pp. 127-43.
15. C. E. Lowell and W. A. Sanders: NASA TN D-6562, 1971.
16. J. R. Johnston and R. L. Ashbrook: NASA TN D-5376, 1969.
17. R. J. Centolanzi, NASA TM X-62015, 1971.
18. F. J. Centolanzi, H. B. Probst, C. E. Lowell, and N. B. Zimmerman: NASA TM X-62092, 1971.
19. D. R. Tenney, C. T. Young, and H. W. Herring: *Met. Trans.,* 1974, vol. 5, pp. 1001-12.
20. J. W. Cloby: MAGIC IV Program, Bell Telephone Lab., Inc., 1971.
21. R. T. Grimley, R. P. Burns, and M. G. Inghram: *J. Chem. Phys.,* 1961, vol. 35, no. 2, pp. 551-54.
22. *Instruction and Operating Procedures for Aerotherm 100 KW Constrictor Arc Heater System,* Aerotherm Corporation, Tech. Narrative Report No. IM-68-1, NASA Contract No. NAS1-7560, 1968.
23. R. T. Grimley, R. P. Burns, and M. G. Inghram: *J. Chem. Phys.,* 1961, vol. 34, no. 2, pp. 664-67.
24. P. G. Dickens, R. Heckingbottom, and J. W. Linnett: *Trans. Faraday Soc.,* 1969, vol. 65, pp. 2235-47.
25. G. C. Fryburg, F. J. Kohl, and C. A. Stearns: *J. Electrochem. Soc.,* 1973, vol. 120, no. 8, p. 234-C.